Pharm Res (2013) 30:435–446
DOI 10.1007/s11095-012-0888-0

RESEARCH PAPER

Squalene-Containing Nanostructured Lipid Carriers Promote Percutaneous Absorption and Hair Follicle Targeting of Diphencyprone for Treating Alopecia Areata

Yin-Ku Lin • Saleh A. Al-Suwayeh • Yann-Lii Leu • Feng-Ming Shen • Jia-You Fang

Received: 5 June 2012 / Accepted: 12 September 2012 / Published online: 16 October 2012

ABSTRACT

Purpose Diphencyprone (DPCP) is a therapeutic agent for treating alopecia areata. To improve skin absorption and follicular targeting nanostructured lipid carriers (NLCs) were developed.

Methods Nanoparticles were characterized by size, zeta potential, molecular environment, differential scanning calorimetry (DSC), and nuclear magnetic resonance (NMR). *In vitro* and *in vivo* skin absorption experiments were performed. Fluorescence and confocal microscopes for imaging skin distribution were used.

Results NLCs with different designs were 208 ~ 265 nm with > 77% DPCP encapsulation. NLCs incorporating a cationic surfactant or more soybean phosphatidylcholine (SPC) showed higher lipophilicity compared to typical NLCs by Nile red emission. All NLCs tested revealed controlled DPCP release; burst release was observed for control. The formulation with more SPC provided 275 μg/g DPCP skin retention, which was greater than control and other NLCs. Intersubject deviation was reduced after DPCP loading into NLCs. Cyanoacrylate skin biopsy demonstrated greater follicular deposition for NLCs with more SPC compared to control. Cationic NLCs but not typical or SPC-containing carriers were largely internalized into keratinocytes. *In vivo* skin retention of NLCs with more SPC was higher than free control. Confocal imaging confirmed localization of NLCs in follicles and intercellular lipids of stratum corneum.

Conclusions This work encourages further investigation of DPCP absorption using NLCs with a specific formulation design.

KEY WORDS alopecia areata · diphencyprone · hair follicles · nanostructured lipid carriers · percutaneous absorption

INTRODUCTION

Alopecia areata (AA) is a chronic inflammatory disorder which attacks hair follicles. The symptom of AA is hair loss on the scalp and also of any hair-bearing skin (1). AA is an autoimmune process involving T cells (2). Topical immunotherapy using contact allergens as therapeutic drugs is used to re-grow hair in AA patients. Among the contact allergens, diphencyprone (DPCP) possesses higher sensitization activity without mutagenic induction (3). DPCP can recruit some T

Y.-K. Lin
School of Traditional Chinese Medicine, Chang Gung University
Kweishan, Taoyuan, Taiwan

Y.-K. Lin
Department of Traditional Chinese Medicine
Chang Gung Memorial Hospital Keelung, Taiwan

S. A. Al-Suwayeh
Department of Pharmaceutics, College of Pharmacy, King Saud University Riyadh, Saudi Arabia

Y.-L. Leu
Natural Products Laboratory, Graduate Institute of Natural Products
Chang Gung University
Kweishan, Taoyuan, Taiwan

F.-M. Shen • J.-Y. Fang (✉)
Pharmaceutics Laboratory, Graduate Institute of Natural Products
Chang Gung University, 259 Wen-Hwa 1st Road
Kweishan, Taoyuan 333, Taiwan
e-mail: fajy@mail.cgu.edu.tw

F.-M. Shen
Chinese Herbal Medicine Research Team
Healthy Aging Research Center, Chang Gung University
Kweishan, Taoyuan, Taiwan

J.-Y. Fang
Department of Cosmetic Science
Chang Gung University of Science & Technology
Kweishan, Taoyuan, Taiwan

cell subpopulations to the diseased region to enhance clearance of putative antigens in follicles (4). However, AA is still difficult to treat with only a ~50% success rate with DPCP (5). Moreover, some patients develop cervical lymphadenopathy and severe dermatitis after DPCP treatment (6). These problems can hopefully be resolved by designing and developing new dosage forms.

Solid lipid nanoparticles (SLNs) and nanostructured lipid carriers (NLCs) are categorized as a new generation of lipid nanoparticles which were developed since the 1990s. SLNs consist of a complete solid lipid matrix, while NLCs are made of a mixture of solid and liquid lipids. SLNs and NLCs are good candidates for drug delivery systems because of their sustained release, targeted efficiency, and lower toxicity than other nanoparticles such as metallic and polymeric systems (7). It was reported that SLNs have some disadvantages, including unexpected aggregation, a gelation tendency, and low drug incorporation efficiency due to their crystalline structure. NLCs were developed to overcome limitations associated with SLNs by increasing the payload and preventing gelation (8). It is possible to enhance drug skin delivery with NLCs, which would be beneficial for DPCP since a 12-month duration is needed to achieve cosmetically acceptable outcomes (9). Since DPCP is very sensitive to light (5), NLCs are ideal storage systems to protect drugs against degradation (10). Drug targeting to hair follicles may improve the therapeutic efficiency and avoid unnecessary local effects on AA. Previous studies (11,12) reported that some nanoparticles can penetrate into follicles. NLCs are a promising nanocarrier for DPCP delivery.

The aim of the present work was to systematically investigate DPCP absorption *via* the skin by encapsulation into NLCs. The formulations were modified to obtain better skin permeation and follicular targeting. Squalene is a predominant component of sebum. Squalene is used as the liquid lipid in nanoparticulate cores since it can easily fuse with the sebum in hair follicles. The structure and physicochemical properties of the nanoparticles were characterized by the particle size, zeta potential, molecular environment, differential scanning calorimetry (DSC), and lipid mobility. The DPCP encapsulation percentage and its permeation/release from NLCs were determined by high-performance liquid chromatography (HPLC). The *in vitro* keratinocyte uptake of nanoparticles was investigated using fluorescence microscopy. Both confocal and fluorescence microscopes were employed to examine *in vivo* skin absorption and follicular delivery of the nanoparticles.

MATERIALS AND METHODS

Materials

DPCP, squalene, cetyl palmitate, Pluronic F68 (PF68), rhodamine 123, and Nile red were purchased from Sigma-Aldrich (St. Louis, MO, USA). 4′,6′-Diamidino-2-phenylindole (DAPI) was supplied by Santa Cruz Biotechnology (Santa Cruz, CA, USA). Hydrogenated soybean phosphatidylcholine (SPC, Phospholipon 80 H®) was obtained from American Lecithin (Oxford, CT, USA). Soyethyl morpholinium ethosulfate (SME, Forestall®) was from Croda Chemical (East Yorkshire, UK). Carboxylic acid-conjugated quantum dots (carboxyl QDs; Qdot® 800 ITK) with an emission maximum at 800 nm were supplied by Invitrogen (Carlsbad, CA, USA). Cellulose membranes (Cellu-Sep® T1, with a molecular weight cutoff of 3500) were purchased from Membrane Filtration Products (Seguin, TX, USA).

Preparation of NLCs

The lipid and water phases of the NLCs were separately fabricated. The lipid phase consisted of 4% (w/v) squalene, 4% cetyl palmitate, and 1% SPC. SME (1%) or additional SPC (1.5%) was added to the lipid phase if necessary. The aqueous phase consisted of double-distilled water and 3.5% PF68. DPCP (0.1%) was incorporated in the lipid phase as the model drug. The two phases were separately heated to 85°C for 15 min. The water phase was subsequently pipetted into the lipid phase and mixed for 5 min. The resultant mixture was further mixed with a high-shear homogenizer (Pro250, Pro Scientific, Monroe, CT, USA) at 12,000 rpm for 20 min. Then a probe-type sonicator (VCX600, Sonics and Materials, Newtown, CT, USA) was used to treat the mixture for 15 min at 35 W. The total volume of the final product was 10 ml.

Particle Size and Zeta Potential

The average diameter and zeta potential of different NLCs were measured by a laser scattering technique (Nano ZS90, Malvern, Worcestershire, UK). The nanocarriers were diluted 100-fold with double-distilled water before the examination. The measurement was repeated three times per sample for three samples.

DPCP Encapsulation Percentage

The efficiency of DPCP loading in the NLCs was determined by an ultracentrifugation method (Optima MAX, Beckman Coulter, Fullerton, CA, USA). Samples were centrifuged at 48,000 x*g* and 4°C for 30 min to separate the incorporated drug from the free form in the external phase. The supernatant and precipitate were withdrawn and analyzed by HPLC (Hitachi 7-series, Tokyo, Japan). A 25-cm-long stainless steel C18 column (Merck, Darmstadt, Germany) with a 4-mm inner diameter was used as the stationary phase. The mobile phase consisted of acetonitrile: water (60: 40). The flow rate was 1 ml/min. The ultraviolet detector was set to a wavelength of 295 nm for detection.

Molecular Environment

The molecular environment (polarity) of the lipid nanoparticles was elucidated by a fluorescence spectrophotometer (F2500, Hitachi) based on the solvatochromism of Nile red. NLCs were prepared with 1 ppm Nile red as described above. The emission fluorescence spectra of Nile red were scanned at 550~700 nm with both slit widths set to 10 nm. The excitation wavelength of the spectrophotometer was set to 546 nm.

DSC

The DSC analysis was conducted using a Q2000 calorimeter (TA Instruments, New Castle, DE, USA). NLCs were lyophilized before the analysis. Lyophilized samples were weighed in aluminum pans, which were then sealed with pinhole-pierced covers. Heating curves were recorded at 0~100°C at a scan rate of 10°C/min under nitrogen.

Nuclear Magnetic Resonance (NMR) Measurements

Mobilization of squalene and cetyl palmitate in NLCs was analyzed by NMR. The nanocarriers were 3-fold diluted with D_2O. Neat squalene and cetyl palmitate were diluted with chloroform-d. Samples were loaded into NMR tubes. ^{1}H-NMR spectra were detected on an Avance 400 spectrometer (Bruker, Bremen, Germany). Line widths of the half-amplitude (Hz) of methyl groups and methylene protons were respectively measured for squalene and cetyl palmitate.

Animals

Female nude mice (ICR-Foxn1nu) and hairy mouse (Balb/c) aged 8 weeks were supplied by the National Laboratory Animal Center (Taipei, Taiwan). The animal experimental protocol was approved by the Institutional Animal Care and Use Committee of Chang Gung University. Mice were housed and handled according to institutional guidelines. Alfalfa-free food (#5058, Labdiet®, Framingham, MA, USA) and water were given *ad libitum*.

In Vitro Percutaneous Absorption

Permeation of DPCP was examined using a Franz cell with nude mouse dorsal skin, hairy mouse dorsal skin, or a cellulose membrane as the permeation barrier. The skin or membrane was mounted between the donor and receptor compartments, with the stratum corneum (SC) layer facing the donor compartment. There was 0.5 ml of drug-containing vehicle in the donor compartment. The receptor medium consisted of 5.5 ml of pH 7.4 citrate-phosphate buffer with 30% (v/v) ethanol. The effective diffusion area was 0.785 cm^2. The stirring rate was set to 600 rpm and the receptor temperature to 37°C. The temperature of the skin surface was maintained at about 32°C after this setting, which was near the *in vivo* status. A 300-μl aliquot was sampled from the receptor at appropriate intervals and then replaced with an equal volume of medium. When the experiment was terminated at 24 h, the skin was removed, cut into pieces, and then homogenized with 1 ml methanol for 5 min to examine DPCP. The resulting mixture was centrifuged at 3,000 rpm for 10 min, and the supernatant was filtered through a polyvinylidene difluoride membrane. The drug concentration was quantified by HPLC.

Differential Stripping/Cyanoacrylate Skin Surface Biopsy

This method was utilized to examine the amount of small-molecule drugs in hair follicles (13). After a 24-h application, the skin was removed from the Franz cell and then the SC was stripped with adhesive tape 20 times. Subsequent to tape stripping, follicular casts were prepared. A drop of superglue (ethyl cyanoacrylate 7004T, 3M, Taipei, Taiwan) was positioned on a glass slide, which was then pressed onto the surface of the stripped skin. The cyanoacrylate polymerized, and the slide was removed with one quick movement after 5 min. The superglue remaining on the slide was scraped off, and then positioned in a test tube containing 2 ml methanol. The tube was shaken for 3 h. The resulting dispersion was vacuumed to evaporate the methanol. The mobile phase was added to samples for the HPLC analysis.

Keratinocyte Internalization by NLCs

To study the cellular uptake by NLCs, quantum dots (14.4 μg/ml) as the fluorescence dye were loaded into NLCs by the same preparation process described in the previous section. Human epidermal neonatal keratinocytes (HEKs-n) were maintained in keratinocyte medium containing 1% keratinocyte growth supplement, 1% penicillin, and 1% streptomycin. Keratinocytes (2×10^5) were seeded in 6-well plates and cultured for 24 h. Then either the free control (in DMSO) or NLCs with quantum dots (1: 100) were added to the plate and incubated for 4 h at 37°C. The medium was removed, and cells were washed twice with phosphate-buffered saline (PBS). DAPI at 100 ng/ml was pipetted into the cell medium to stain cell nuclei. Cellular uptake of quantum dots was imaged under an inverted fluorescence microscope (IX81, Olympus, Tokyo, Japan). The excitation and emission wavelengths were respectively set to 405 and 800 nm.

In Vivo Percutaneous Absorption

A glass cylinder with an available area of 0.785 cm^2 was fixed onto the dorsal skin of nude mouse with glue. The cylinder was filled with the vehicle for DPCP (0.2 ml). The application time for the permeants was 6 h. Animals were sacrificed, and the treated skin area was excised to determine the drug concentration in the skin. The extraction procedure for DPCP was the same with that performed in the *in vitro* experiment.

Fluorescence Microscopic Imaging

Rhodamine 123 (0.03%) in propylene glycol (PG)/water (3: 7) or NLCs were used as the dye in this study to observe the nude mouse skin structure and fluorescence distribution in the skin. After *in vivo* percutaneous absorption application (6 h), animals were sacrificed, and specimens of the applied skin area were excised. Each skin sample was cut vertically, embedded in OCT, and frozen at −70°C. Samples were subsequently sectioned in a cryostat microtome and mounted with glycerin and gelatin. Slices were examined with an inverted microscope (IX81, Olympus) using respective filter sets at 450 ~ 490 and 515 ~ 565 nm for excitation and emission. Slices were also stained with hematoxylin and eosin (H&E) for observation under light microscopy.

Confocal Laser Scanning Microscopy (CLSM)

The skin was excised to examine fluorescence signals of rhodamine 123 by CLSM after *in vivo* percutaneous absorption (6 h). The skin surface was washed with methanol to remove residual permeants. The skin thickness was optically scanned at 5-μm increments through the Z-axis of a Leica TCS SP2 confocal microscope (Wetzlar, Germany). Optical excitation and emission wavelengths were respectively set to 488 and 500 ~ 535 nm. Images were taken by summing 10 fragments at various skin depths from the skin surface.

Statistical Analysis

The analysis was carried out using an unpaired Student's *t*-test or analysis of variance (ANOVA). A 0.05 level of probability ($p < 0.05$) was accepted as statistically significant.

RESULTS

Particle Size, Zeta Potential, and DPCP Encapsulation Percentage

Table I summarizes the particle size, zeta potential, and drug encapsulation of various NLCs. F1 was the standard formulation with PF68 (3.5%) and SPC (1%) as the emulsifiers. The F2 and F3 formulations additionally incorporated a cationic surfactant (SME) and excess SPC (1.8%), respectively. All nanosystems revealed a small diameter ranging about 210 ~ 260 nm, which remained in the nanometer level. Standard NLCs (F1) had a mean size of 208 nm. The particulate size increased to 265 nm after loading SME (F2). Extra SPC incorporation (F3) slightly increased ($p < 0.05$) the diameter to 236 nm. Zeta potential measurements demonstrated a negative charge of F1 at −55 mV. The zeta potential changed from negative to positive (54 mV) after adding SME. It was found that further addition of SPC from 1% to 1.8% resulted in no change ($p > 0.05$) in the surface charge of particles. An important issue for nanocarriers as drug delivery systems is the encapsulation efficiency of the drug. The loading capacity of DPCP in lipid nanoparticles is illustrated in Table I. F1 showed an encapsulation value of 77%. The presence of SME and excess SPC in the carriers was useful in increasing the entrapment capacity from 77% to 86%.

Table I Characterization of the Nanostructured Lipid Carriers by Particle Size, Zeta Potential, and Diphencyprone

Formulation	Size (nm)	Zeta potential (mV)	Encapsulation percentage (%)
F1	207.8 ± 1.3	−55.1 ± 1.0	76.9 ± 1.0
F2	264.9 ± 3.9	54.4 ± 0.4	85.6 ± 4.6
F3	236.3 ± 3.2	−52.8 ± 4.7	85.8 ± 1.8

Each value represents the mean ± SD ($n = 3$)

Molecular Environment

Nile red is a solvatochromic dye. Its fluorescence is strengthened in more-lipophilic dispersions. It is a marker of fluorescence emissions which can change with environmental polarity after nanoparticulate inclusion. The spectra of emissions from Nile red in the nanosystems are depicted in Fig. 1. Nile red was strongly fluorescent in methanol, with a maximum intensity near 620 nm. The encapsulation by NLCs significantly quenched the fluorescence emission. F1 demonstrated the weakest Nile red emission, followed by F3 and F2.

DSC

The crystallization and thermal characteristics of the inner cores of the nanoparticles were examined by DSC. Figure 2 shows the melting process of bulk cetyl palmitate and NLCs after freeze-drying. Bulk cetyl palmitate revealed a sharp peak melting point at 55.66°C. The melting peaks of cetyl

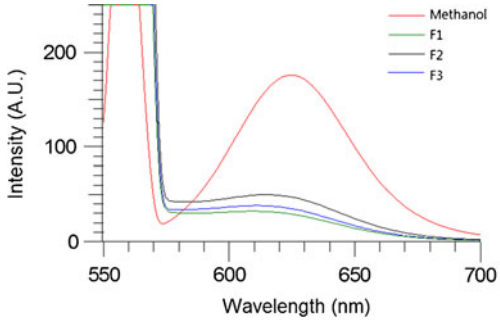

Fig. 1 Fluorescence emission profiles of Nile red in methanol and nanostructured lipid carriers (NLCs). The emission fluorescence spectra of Nile red were scanned at 550~700 nm with both slit widths set to 10 nm.

palmitate in NLCs decreased by ~13°C. The melting enthalpies in NLCs were 97~109 J/g, which were much lower ($p<0.05$) than that of the bulk material (229 J/g). The different types of NLCs did not appear to greatly influence the DSC measurements.

NMR Measurements

The mobility of squalene and cetyl palmitate in particulate cores was investigated by proton NMR. The NMR line width of the signals is summarized in Table II. The respective line widths obtained for neat squalene and cetyl palmitate were 5.34 and 4.59 Hz. Widths greatly increased when encapsulated into lipid nanocarriers. Squalene in NLCs showed widths of 10.39~11.89 Hz, values 2-times higher than the bulk material. The width of the squalene signal showed an increasing trend of F3>F2>F1. A similar profile was observed for cetyl palmitate, with F3 exhibiting the greatest increase of 6.8-fold.

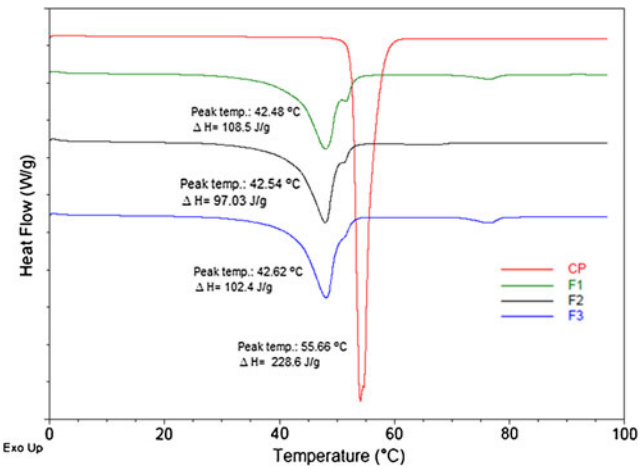

Fig. 2 DSC profiles of the melting process of bulk cetyl palmitate and the cetyl palmitate peak in nanostructured lipid carriers (NLCs).

Table II Linewidth at Half-Amplitude of Nuclear Magnetic Resonance Signals as a Feature of Immobilized Chemical Groups

Formulation	Linewidth of squalene	Linewidth of cetyl palmitate
Control (neat)	5.34	4.59
F1	10.39	20.82
F2	11.82	23.38
F3	11.89	30.99

In Vitro Percutaneous Absorption

The skin permeation of DPCP was evaluated *in vitro*. We first examined DPCP retention within the skin at 24 h for possible skin targeting of lipid nanoparticles. The control vehicle was water with 30% PG. Another control vehicle used in this experiment was acetone, which is commonly used as a DPCP medium in the clinic. As shown in Table III, control dispersions of PG/water and acetone exhibited nude mouse skin accumulations of 171 and 207 μg/g, respectively. The intersubject variations of the control groups were larger according to the mean and standard deviation (SD) values, especially for acetone. F1 and F3 revealed higher skin deposition levels of DPCP ($p<0.05$) compared to the PG/water vehicle, whereas there was no significant difference ($p>0.05$) between values of F2 and PG/water. Maximum skin retention was obtained when the permeant was loaded in NLCs with a greater amount of SPC (F3). Hairy mouse skin was also used as a permeation barrier in Table III. Most of the tested carriers showed a lower skin deposition in hairy mouse skin than nude mouse skin, except for cationic NLCs (F2). The ratio between skin deposition levels with nude mouse and hairy mouse ($ratio_{hairy/nude}$) was calculated as an indicator of follicular targeting. It was apparent that all NLCs showed a greater ratio compared to the control groups. F2 demonstrated the highest ratio (1.48) among all of the NLCs tested.

Figure 3a illustrates DPCP accumulation in receptors of the Franz cell. Detection of the permeant in the receptor may indicate its presence in deeper skin strata or systemic circulation if used *in vivo*. The penetration kinetics of all formulations were approximately similar to each other. A relative DPCP burst was detected for the PG/water vehicle. The penetration kinetics of the free control was not in a zero-order fashion. It was observed that F1 and F3 showed controlled penetration which obeyed a zero-order equation. The amount of DPCP that had permeated across nude mouse skin by 24 h is shown in Table IV. Values across hairy mouse skin are also given for comparison. There was no significant difference ($p>0.05$) between the levels of nude mouse skin and hairy mouse skin for the control, F1, or F3 groups. The amount permeating across hairy mouse skin was lower ($p<0.05$) than that across nude mouse skin for F2, which showed a $ratio_{hairy/nude}$ value of 0.76. It is important to explore the release kinetics and

Table III *In Vitro* Skin Retention ($\mu g/g$) of Diphencyprone in Nude Mouse and Hairy Mouse Skins

Formulation	Nude mouse	Hairy mouse	$Ratio_{hairy/nude}$
Control (PG)	171.10 ± 27.88	103.41 ± 19.91	0.60
Control (acetone)	207.34 ± 171.63	123.26 ± 83.62	0.59
F1	195.82 ± 16.84	165.86 ± 29.65	0.85
F2	156.08 ± 11.21	230.84 ± 16.12	1.48
F3	274.67 ± 22.85	266.52 ± 31.22	0.97

Each value represents the mean ± SD (n=4).

Table IV *In Vitro* Permeated Amount at 24 h ($\mu g/cm^2$) of Diphencyprone in Nude Mouse and Hairy Mouse Skins

Formulation	Nude mouse	Hairy mouse	$Ratio_{hairy/nude}$
Control (PG)	243.30 ± 43.50	256.10 ± 50.25	1.05
Control (acetone)	260.07 ± 140.86	180.86 ± 134.60	0.70
F1	282.01 ± 37.68	289.40 ± 31.89	1.03
F2	306.24 ± 39.26	233.76 ± 21.76	0.76
F3	283.13 ± 35.63	282.34 ± 12.96	1.00

Each value represents the mean ± SD (n=4)

mechanisms when developing a prolonged-release system. Results of the release of DPCP across the cellulose membrane are given in Fig. 3b. The release kinetics increased in the order of F1 > F3 > F2 > control. Drug was rapidly released from the free control in the initial stage, followed by suspended delivery after 8 h. NLCs continually released DPCP until the end of the experiment (24 h). The amount of NLCs released exceeded that of the control vehicle in the late stage.

Differential Stripping/Cyanoacrylate Skin Surface Biopsy

In order to examine the effect of NLCs on the appendageal pathway, the amount of DPCP in hair follicles was detected by a combination of stripping and cyanoacrylate casting. Recovery of the drug from casts is shown in Fig. 4. After a 24-h administration time, 389 ng/g of DPCP was recovered from follicles of control skin (PG/water). The increase in the follicular amount from conventional NLCs (F1) was not significant ($p > 0.05$). Improved DPCP targeting to follicles ($p < 0.05$) was observed when the drug was loaded in the F2 and F3 formulations. A statistical analysis demonstrated no difference ($p > 0.05$) between follicular amounts obtained with the F2 and F3 formulations. Both NLCs increased follicular uptake by about 2-fold compared to the aqueous control.

Keratinocyte Internalization by NLCs

To check whether the nanoparticles were endocytosed by keratinocytes, the possible internalization of NLCs was visualized by fluorescence microscopy as shown in Fig. 5. The DMSO control with fluorescence dye, QDs, revealed no signal other than DAPI-stained nuclei (Fig. 5a). A negligible or weak red fluorescence was observed in the photographs of keratinocytes treated with F1 and F3 (Fig. 5b, d). A higher intensity of signaling was exhibited in cells treated with cationic nanoparticles (F2) compared to the others (Fig. 5c), suggesting a better internalization ability. The QDs in F2 emitted fluorescence within the cytoplasm and near nuclei.

In Vivo Percutaneous Absorption

The *in vivo* skin retention of DPCP was examined after 6-h administration on nude mouse dorsal skin. As depicted in Fig. 6, the nanocarriers with a greater amount of SPC (F3) exhibited the greatest accumulation ($p < 0.05$) within the skin,

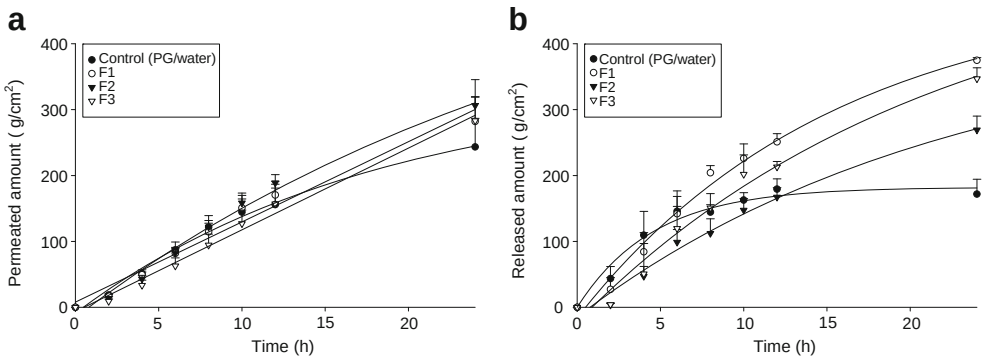

Fig. 3 *In vitro* permeated amount-time profiles of diphencyprone (DPCP) across (**a**) nude mouse skin and (**b**) cellulose membranes from the free control (PG/water) and nanostructured lipid carriers (NLCs). Each value represents the mean and S.D. (n=4).

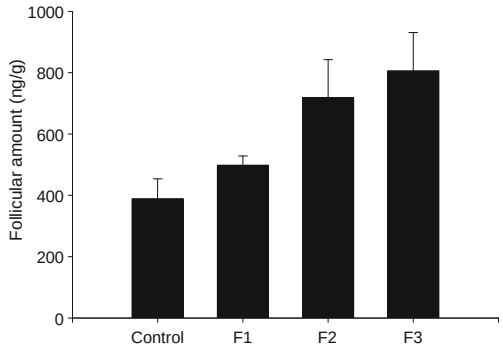

Fig. 4 Diphencyprone (DPCP) amount in hair follicles (ng/g) of nude mouse skin treated after *in vitro* skin absorption (24 h) of the free control (PG/water) and nanostructured lipid carriers (NLCs). Each value represents the mean and S.D. (n=4).

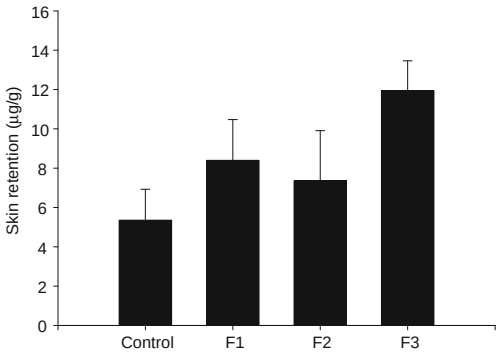

Fig. 6 *In vivo* skin retention of diphencyprone (DPCP) in nude mouse skin after *in vivo* topical application of free control (PG/water) and nanostructured lipid carriers (NLCs) for 6 h. Each value represents the mean and S.D. (n=4).

followed by the conventional (F1) and cationic (F2) formulations. The control group showed the least DPCP absorption. This order was the same as that of *in vitro* skin retention (Table III). There was no significant difference ($p>0.05$) among values of the control vehicle, F1, and F2. Following application of F3, DPCP deposition increased by about 2-fold over the uptake achieved by PG and the water vehicle.

Fluorescence Microscopic Imaging

Fluorescence imaging was employed to observe the dye distribution from PG/water and NLCs into nude mouse skin. Figure 7a demonstrates images of vertical skin sections with no treatment. The left panel is fluorescence imaging. This imaging is merged with H&E staining of the skin morphology as shown in the right panel. Light microscopy indicated no observable damage of the entire skin for any formulation tested. No fluorescence signal from the blank skin at the set wavelength ranges was visualized, suggesting a low autofluorescence of the skin itself. The skin distribution of the dye was largely affected by the carriers. After administration of PG/water containing rhodamine 123, green fluorescence was distributed in the epidermis and hair follicles in a non-continuous manner (Fig. 7b). A similar distribution was observed for F1-treated skin as shown in Fig. 7c. Fluorescence was only detectable on the skin surface, and no signal was shown in deeper strata. Figure 7d indicates increased dye penetration into skin layers when administering cationic nanoparticles (F2) compared to F1 and the control. The merged picture in the right panel of Fig. 7d demonstrates that the signals were mainly located in follicular regions. As depicted in Fig. 7e, there was widespread accumulation of green fluorescence throughout the skin layers treated by F3. The dye penetrated much more deeply into the skin than with the other carriers. The fluorescence was deposited homogeneously and continuously on the skin surface. The superimposed image shows that fluorescence staining accumulated in hair follicles, which could extend dye transport to the dermis.

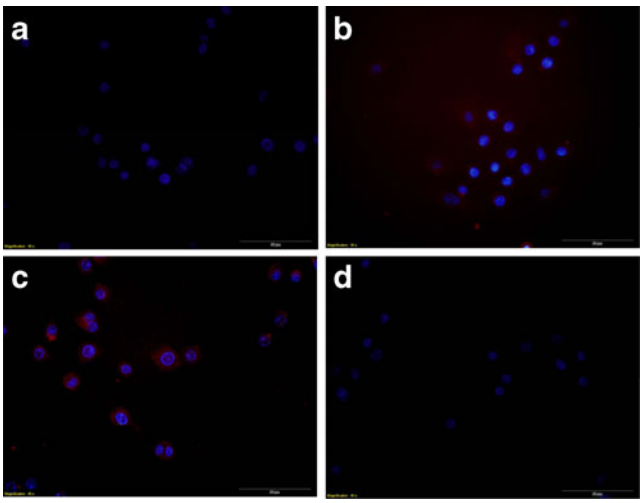

Fig. 5 Fluorescence microscopic images of human epidermal keratinocyte internalization by (**a**) the free control (PG/water), (**b**) typical nanostructured lipid carriers (NLCs, F1), (**c**) cationic NLCs (F2), and (**d**) NLCs with excess SPC (F3) after a 4-h incubation.

CLSM

Dye accumulation in the skin was also examined using CLSM. Figure 8a represents the image (630x) from intact skin which illustrates the collective emission in tissues scanned at 5-µm increments from the skin surface. Non-treated skin exhibited no fluorescence in the detection range. No significant deposition of a green signal into the skin was seen for the PG/water control (Fig. 8b). Some fluorescence was detected in hair shafts. A much higher intensity was noted in F1-treated skin (Fig. 8c). The dye tended to assemble along the edges of corneocytes. This suggests that the diffusion route across the SC was intercellular. Figure 8c also displays the location of fluorescence in the vicinity of follicles and hair shafts. Figure 8d shows that the dye distribution was concentrated along follicles and

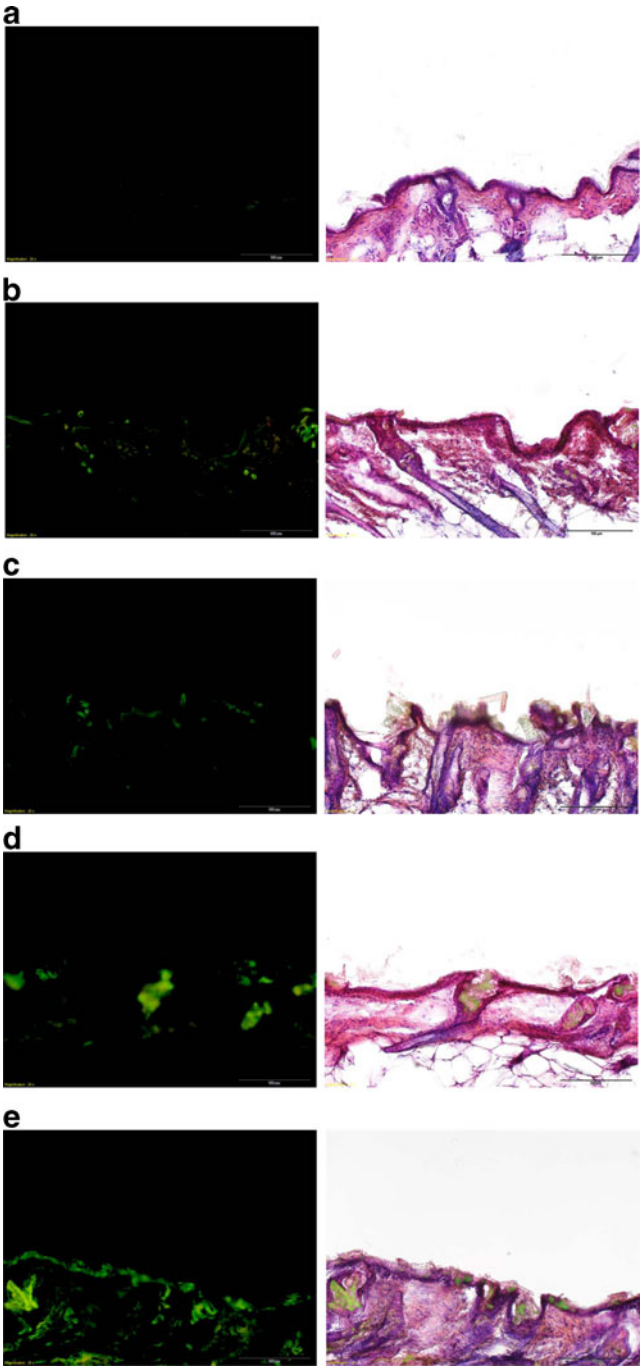

Fig. 7 Fluorescence microscopic images of nude mouse skin with (**a**) non-treatment or after *in vivo* topical application of (**b**) the free control (PG/water), (**c**) typical nanostructured lipid carriers (NLCs, F1), (**d**) cationic NLCs (F2), and (**e**) NLCs with excess SPC (F3). The left panel is the fluorescence image detected at 450~490 and 515~565 nm for excitation and emission; the right panel is the superimposed picture of the fluorescence and H&E-stained images.

perifollicular areas after treatment with cationic nanoparticles (F2). The fluorescence was shown to approach the epidermis *via* lipid bilayers of the SC. The intensity of fluorescence was much higher for nanocarriers with a greater amount of SPC (F3) than for F1 and F2 (Fig. 8e). There was widespread distribution of the dye mainly located in follicles, hair shafts, and intercellular regions.

DISCUSSION

Three formulations were developed for examination in this study. In addition to typical NLCs (F1), SME (F2) was added to produce a positive surface charge in order to increase electrostatic interactions between the negatively charged skin surface and nanoparticles. Since phospholipids in liposomes can promote vesicle entrance into hair follicles (14), an excess of SPC was loaded in the NLCs for follicular delivery. Compared to F1, the additional SME and SPC residing in the particulate shell produced a larger surface area, thus increasing the particle diameter. The 20% of components other than phosphatidylcholine in SPC, such as phosphatidylserine, phosphatidic acid, and phosphatidylinositol, contributed to the negative zeta potential (15). Cationic SME significantly reversed the negative charge to a positive charge on the particulate surface. The zeta potential can be a predictor of colloidal stability (16). A sufficient zeta potential of>|30| mV provides electric repulsion to avoid particle fusion (17). Our nanocarriers fit this criterion. Moreover, PF68 supplied additional steric repulsion for nanoparticulate stability (18).

A higher melting temperature and enthalpy suggest an ordered and rigid lattice arrangement and *vice versa* (19). Melting point depression and peak broadening in DSC were observed after cetyl palmitate was incorporated in the nanocarriers. This shift was ascribed to a distortion of the crystalline lattice and the blending of liquid and solid lipids (20). However, the existence of peaks for the nanoparticles may indicate a solid state of the lipid matrix at room temperature. Imperfections in the lattice structure of NLCs are preferred in order to accommodate DPCP molecules. A high entrapment efficiency of >77% was shown for NLCs. DPCP has high lipophilicity (partition coefficient, log P=3.85) which makes it an excellent candidate for lipid nanoparticle encapsulation. SME and SPC increased the nanoparticulate lipophilicity according to Nile red emissions. DPCP was easily intercalated in the lipid matrices of F2 and F3 with high affinity, resulting in greater entrapment compared to F1. The NMR line width at half-amplitude of the signal represents the mobility of the materials. Broader and smaller signals respectively indicate restricted mobility and potent interactions (21). The formulation with excess SPC (F3) showed a broader signal than the other NLCs, indicating confined mobilization of the lipids in the cores after inclusion of SPC. Although SME and additional SPC did not affect the extent of crystalline lattice formation in the inner matrix, mobilization of materials in the inner cores was modulated by these emulsifiers which resided on the particulate surface.

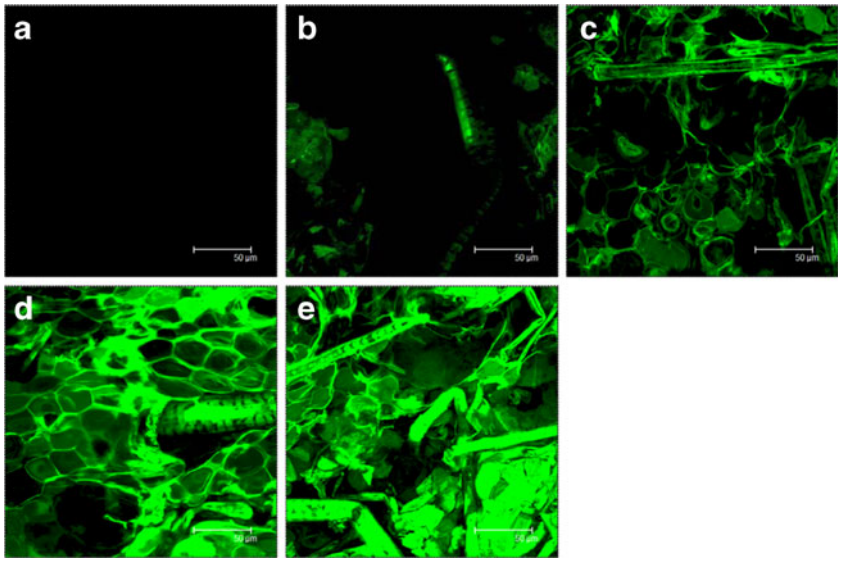

Fig. 8 Confocal micrographs of nude mouse skin at an original magnification of 630x after (**a**) non-treatment, or the *in vivo* topical application of (**b**) the free control (PG/water), (**c**) typical nanostructured lipid carriers (NLCs, F1), (**d**) cationic NLCs (F2), and (**e**) NLCs with excess SPC (F3) for 6 h. The image is a summary of 10 fragments at various skin depths.

The experimental results of nude mouse skin showed that most of the NLCs increased DPCP skin accumulation, a fact that categorizes the permeant as a topical drug, compared to the PG/water control. In clinical situations, acetone is usually used as the vehicle for DPCP application (3).

Acetone demonstrated a greater DPCP deposition in skin than did the PG/water control, which may have been due to rapid disruption of SC lipids. A very large intersubject variation was observed with the acetone group. This variation was expected since the response rate of DPCP therapy greatly varies at 4%~85% (4,22). There was a relatively low inter-individual deviation for NLCs, indicating a superior control of DPCP delivery than for the free control.

Retention of DPCP by nude mouse skin from NLCs showed a trend of F3>F1>F2. Previous studies (23,24) reported that intact nanoparticles penetrated the SC with difficulty. NLCs should have had some effects on absorption enhancement other than permeation in intact forms. DPCP amounts of >75% were dispersed in <10% of the volume of nanosystems according to the encapsulation percentage. NLC particles can easily adhere to the skin surface for direct drug diffusion with a great concentration gradient (8). Although it is difficult for intact particles to penetrate into the SC, uptake of the components is possible (25,26). The lipid nanocarriers exchanged lipids with SC lipids, thus compromising the barrier function (27). Another possible mechanism is the skin hydration effect due to occlusion of NLCs (28), which may enlarge the intercellular route of the SC. Among all NLCs, the formulation with excess SPC (F3) exhibited the greatest DPCP accumulation in the skin. SPC can reduce the surface tension of colloids, allowing them to have closer contact with the skin surface (29). SPC also fuses with SC lipids to loosen the lamellar integrity (30) which has an enhancing effect. An abundant amount of SPC in NLCs increased the lipophilicity of the particles. This may have resulted in effortless fusion with SC lipids compared to F1.

The DPCP released from NLCs had some impacts on skin retention. Cationic NLCs showed lower drug release compared to the other formulations, retarding DPCP partitioning into the SC. Lipophilic DPCP molecules easily associated with the lipid matrix to retard permeant escape from the lipid cores. Another possibility for the slow release of cationic NLCs was the larger size compared to the other NLCs. The total surface area decreases following an increase in particulate size where the release process occurs (31). Drug release in the control group was very low, because DPCP could not completely dissolve in PG/water. Because DPCP totally solubilized in NLCs, regular and continuous release was achieved to produce greater absorption in a dissolved form.

With respect to the pathology of AA, inflammatory cells such as T cells and macrophages are found inside and near hair bulbs. Hair follicles are important for absorption of large molecules and nanoparticles (24). It was assumed that targeting DPCP to follicles could be accomplished by lipid nanoparticles. Follicular density is an essential anatomical factor for judging drug penetration *via* the skin. Undeveloped follicles exist in nude mouse skin, which are found to be covered by desquamated corneocytes, dry sebum, and cell debris (32). We used hairy mouse skin as another diffusion barrier to explore the role of follicles in DPCP delivery. According to the $\text{ratio}_{\text{hairy/nude}}$ of skin retention, NLCs exhibited a higher level compared to control groups. This indicates a higher DPCP accumulation in hair follicles. Cationic NLCs (F2) were the carriers with the highest follicular accumulation. On the other hand, cationic NLCs showed the lowest value of the $\text{ratio}_{\text{hairy/nude}}$ for the amount that penetrated across the skin. This formulation may enhance follicular targeting and minimize penetration through the skin. The skin itself and follicles possess negative charges on their surface (33). Cationic nanoparticles interact with the follicular surface due to electrostatic attraction, although

the overall DPCP skin retention did not increase because of this interaction. High flexibility of nanoparticles can be a positive factor for diffusion into narrow slots between a hair shaft and the root sheath (11,33). DSC results showed a great reduction of nanoparticulate rigidity, favoring their entrance into follicles. The elastic property may be insufficient to affect the delivery through inter- and intracellular routes.

The efficiency of NLCs for follicular targeting was also examined by combining stripping and cyanoacrylate surface biopsy techniques. The DPCP amount in follicles was low for the free control. This was possible since hair follicles are intact and not damaged in AA patients (34). NLCs promoted DPCP retention in follicles with a trend of F3≥F2>F1. Conventional nanocarriers (F1) did not show superior targeting compared to the control. This suggests the importance of formulation modification to exert an enhancing effect.

It is still unknown whether lipid nanoparticles enhanced DPCP absorption predominantly by an intercellular lipid route or by cellular uptake. Keratinocyte internalization of nanoparticles may become evident when they permeate into the epidermis (35). Lipid nanocarriers can be delivered into cells by endocytosis and lipid-mediated fusion (36). We propose that NLCs likely fused with cell membranes and then released the dye into the cytosol. The results showed the greatest uptake for F2, indicating efficient internalization of cationic nanoparticles. The failure of cellular uptake is usually attributed to anionic nanoparticles which are repelled by negatively charged cell membranes. Cationic nanoparticles are thought to easily interact with cell plasma membranes, subsequently enhancing their uptake into cells (37). The skin retention of F2 not surpassing those of the other NLCs suggested a less-important capacity of keratinocyte uptake for NLC delivery into the skin. The cell uptake study elucidated the pathways of DPCP absorption from NLCs.

In the *in vivo* percutaneous absorption study, it was demonstrated that F3 delivered a higher DPCP deposition within the skin than the other formulations. This result coincided with the profile of *in vitro* percutaneous absorption. The fluorescence imaging of vertical skin slices showed a continuous distribution of fluorescence in the epidermis after applying F3. Nevertheless, we did not observe much fluorescence in the epidermis for F1 or F2. This may have contributed to the greater DPCP accumulation from nanosystems with excess SPC. Previous studies (11,38) deduced that nanoparticles can closely contact with furrows between corneocytes and form intercellular deposits, which favor accumulation, allowing increased and sustained permeant delivery. More SPC may have accelerated this process and increased lipid exchange with SC components. Both the SC and epidermal-dermal junctions are diffusion barriers for permeants. It is difficult for lipid nanoparticles to deeply penetrate the skin *via* intercellular pathways. An efficient pathway for nanoparticles to penetrate into deeper strata is follicular delivery. Fluorescence imaging revealed significant accumulation in follicles for F2 and F3. CLSM is an efficient tool to evaluate the distribution of dyes in follicles (39). CLSM imaging also displayed an intense fluorescence in hair shafts and follicles.

Squalene is a predominant ingredient of sebum. Follicles are generally active in sebum secretion and hair growth. There are still 30% of follicles which are inactive and closed due to dry sebum (40). Nude mouse skin has follicles with an undeveloped and inactive nature. Squalene in NLCs may open up follicles with dry sebum. Squalene also easily fuses with sebum in active follicles. However, this hypothesis cannot explain the superior accumulation of F2 and F3 than F1. The follicular penetration may be especially beneficial for lipophilic nanoparticles such as F2 and F3 to enrich the sebum. Corneocytes in follicles are small and crumbly, indicating a deficient permeation barrier (32). Follicular penetration is an easy way to allow drug absorption after nanoparticulate entrance into the infundibulum of follicles. Hair follicles contain specific populations of cell, especially immune cells such as mast cells and T cells, which represent an important target region. A leading action mechanism of DPCP is induction of apoptosis in perifollicular lymphocytes and a shift in lymphocyte location from perifollicular to interfollicular regions (26). CLSM profiles revealed strong fluorescence in intercellular areas near follicles after treatment with NLCs. This is advantageous for DPCP therapy.

Frum *et al.* (41) concluded that drugs with log *P* of >2 produce minor entrance into follicles. The log *P* of DPCP (3.85) caused unfavorable capture by follicles. NLCs, especially F3, enhanced follicular targeting of DPCP to accelerate its transport due to the reduced barrier character of follicles. Follicles also provide a pathway for a long-term reservoir (42). Thus sustained and prolonged therapy can be obtained. DPCP absorption should be deep enough to reach immune cells. It was found that F3 penetrating to deeper skin strata resulted in an enhanced response to AA therapy.

CONCLUSION

Many patients suffer from AA nowadays. Various agents have been used to treat AA, but none are curative. Development of new drugs and formulations is urgently needed. We successfully prepared NLCs loaded with squalene for this goal. Follicular delivery is a major route for AA treatment. Squalene-containing NLCs enhanced both percutaneous absorption and follicular penetration of DPCP delivery. The intersubject variation in DPCP absorption was significantly reduced by application of NLCs compared

to the control vehicles (PG/water and acetone). The lipid nanocarriers with an excess amount of SPC (F3) exhibited the most promising characteristics among the NLCs tested. Increased DPCP skin accumulation and controlled release were achieved with this system. NLCs with a greater amount of SPC improved DPCP delivery into follicles, which may have been due to fusion with sebum or opening of inactive follicles. Cationic NLCs (F2) also showed selective absorption into follicles because of their ability to increase follicular penetration, whereas the total skin deposition and intercellular route were minimized. From the experimental results of this study, it is anticipated that NLCs will provide a feasible alternative for formulating DPCP to produce a controlled and modern delivery system. The knowledge involved in follicular drug targeting triggered by NLCs can be extended to the therapy of other follicle-related diseases including acne and androgenetic alopecia.

ACKNOWLEDGMENTS AND DISCLOSURES

This project was supported by the National Plan for Science and Technology in the Kingdom of Saudi Arabia (grant number: 10-NAN1030-02).

REFERENCES

1. MacDonald Hull SP, Wood ML, Hutchinson PE, Sladden M, Messenger AG. Guidelines for the management of alopecia areata. Br J Dermatol. 2003;149:692–9.
2. Pazoki-Toroudi H, Ajami M, Babakoohi S, Khaki L, Habibey R, Akhiani M, *et al.* Effects of diphencyprone on expression of Bcl-2 protein in patients with alopecia areata. Immunopharmacol Immunotoxicol. 2010;32:422–5.
3. El-Zawahry BM, Bassiouny DA, Khella A, Zaki NS. Five-year experience in the treatment of alopecia areata with DPC. J Eur Acad Dermatol Venereol. 2010;24:264–9.
4. Avgerinou G, Gregoriou S, Rigopoulos D, Stratigos A, Kalogeromitros D, Katsambas A. Alopecia areata: topical immunotherapy treatment with diphencyprone. J Eur Acad Dermatol Venereol. 2008;22:320–3.
5. Alkhalifah A, Alsantali A, Wang E, McElwee KJ, Shapiro J. Alopecia areata update. Part II. Treatment. J Am Acad Dermatol. 2010;62:191–202.
6. Pires MC, Martins JM, Montealegre F, Gatti FR. Vitiligo after diphencyprone for alopecia areata. Dermatol Res Pract. 2010;2010:171265.
7. Müller RH, Radtke M, Wissing SA. Solid lipid nanoparticles (SLN) and nanostructured lipid carriers (NLC) in cosmetic and dermatological preparations. Adv Drug Deliv Rev. 2002;54:S131–55.
8. González-Mira E, Nikolić S, García ML, Egea MA, Souto EB, Calpena AC. Potential use of nanostructured lipid carriers for topical delivery of flurbiprofen. J Pharm Sci. 2011;100:242–51.
9. Wiseman MC, Shapiro J, MacDonald N, Lui H. Predictive model for immunotherapy of alopecia areata with diphencyprone. Arch Dermatol. 2001;137:1063–8.
10. Puglia C, Bonina F, Rizza L, Blasi P, Schoubben A, Perrotta R, *et al.* Lipid nanoparticles as carrier for octyl-methoxycinnamate: *in vitro* percutaneous absorption and photostability studies. J Pharm Sci. 2012;101:301–11.
11. Baroli B, Ennas MG, Loffredo F, Isola M, Pinna R, López-Quintela MA. Penetration of metallic nanoparticles in human full-thickness skin. J Invest Dermatol. 2007;127:1701–12.
12. Zhang LW, Monteiro-Riviere NA. Assessment of quantum dot penetration into intact, tape-stripped, abraded and flexed rat skin. Skin Pharmacol Physiol. 2008;21:166–80.
13. Teichmann A, Jacobi U, Ossadnik M, Richter H, Koch S, Sterry W, *et al.* Differential stripping: determination of the amount of topically applied substances penetrated into the hair follicles. J Invest Dermatol. 2005;125:264–9.
14. Betz G, Imboden R, Imanidis G. Interaction of liposome formulations with human skin *in vitro*. Int J Pharm. 2001;229:117–29.
15. Wen CJ, Zhang LW, Al-Suwayeh SA, Yen TC, Fang JY. Theranostic liposomes loaded with quantum dots and apomorphine for brain targeting and bioimaging. Int J Nanomed. 2012;7:1599–611.
16. Hsu SH, Wen CJ, Al-Suwayeh SA, Chang HW, Yen TC, Fang JY. Physicochemical characterization and *in vivo* bioluminescence imaging of nanostructured lipid carriers (NLCs) for targeting the brain: apomorphine as a model drug. Nanotechnology. 2010; 21:405101.
17. Chen H, Chang X, Du D, Liu W, Liu J, Weng T, *et al.* Podophyllotoxin-loaded solid lipid nanoparticles for epidermal targeting. J Contr Rel. 2006;110:296–306.
18. Zimmermann E, Müller RH. Electrolyte- and pH-stabilities of aqueous solid lipid nanoparticle (SLN®) dispersions in artificial gastrointestinal media. Eur J Pharm Biopharm. 2001;52:203–10.
19. Müller RH, Runge SA, Ravelli V, Thünemann AF, Mehnert W, Souto EB. Cyclosporine-loaded solid lipid nanoparticles (SLN®): drug-lipid physicochemical interactions and characterization of drug incorporation. Eur J Pharm Biopharm. 2008;68:535–44.
20. Wang JJ, Liu KS, Sung KC, Tsai CY, Fang JY. Lipid nanoparticles with different oil/fatty ester ratios as carriers of buprenorphine and its prodrugs for injection. Eur J Pharm Sci. 2009;38:138–46.
21. Schubert MA, Harms M, Müller-Goymann CC. Structural investigations on lipid nanoparticles containing high amounts of lecithin. Eur J Pharm Sci. 2006;27:226–36.
22. Happle R. Diphencyprone for the treatment of alopecia areata: more data and new aspects. Arch Dermatol. 2002;138:112–3.
23. Gopee NV, Roberts DW, Webb P, Cozart CR, Siitonen PH, Latendresse JR, *et al.* Quantitative determination of skin penetration of PEG-coated CdSe quantum dots in dermabraded but not intact SKH-1 hairless mouse skin. Toxicol Sci. 2009;111:37–48.
24. Baroli B. Penetration of nanoparticles and nanomaterials in the skin: fiction or reality? J Pharm Sci. 2010;99:21–50.
25. Lombardi Borgia S, Regehly M, Sivaramakrishnan R, Mehnert W, Korting HC, Danker K, *et al.* Lipid nanoparticles for skin penetration enhancement–correlation to drug localization within the particle matrix as determined by fluorescence and parelectric spectroscopy. J Contr Rel. 2005;110:151–63.
26. Schäfer-Korting M, Mehnert W, Korting HC. Lipid nanoparticles for improved topical application of drugs for skin diseases. Adv Drug Deliv Rev. 2007;59:427–43.
27. Desai P, Patlolla RR, Singh M. Interaction of nanoparticles and cell-penetrating peptides with skin for transdermal drug delivery. Mol Membr Biol. 2010;27:247–59.
28. Pardeike J, Hommoss A, Müller RH. Lipid nanoparticles (SLN, NLC) in cosmetic and pharmaceutical dermal products. Int J Pharm. 2009;366:170–84.
29. Wang JJ, Liu KS, Sung KC, Tsai CY, Fang JY. Skin permeation of buprenorphine and its ester prodrugs from lipid nanoparticles:

lipid emulsion, nanostructured lipid carriers, and solid lipid nanoparticles. J Microencapsul. 2009;26:734–47.
30. Abdel-Mottaleb MMA, Neumann D, Lamprecht A. Lipid nanocapsules for dermal application: a comparative study of lipid-based *versus* polymer-based nanocarriers. Eur J Pharm Biopharm. 2011;79:36–42.
31. Liu KS, Wen CJ, Yen TC, Sung KC, Ku MC, Wang JJ, *et al.* Combined strategies of apomorphine diester prodrugs and nanostructured lipid carriers (NLCs) for efficient brain targeting. Nanotechnology. 2012;23:095103.
32. Knorr F, Lademann J, Patzelt A, Sterry W, Blume-Peytavi U, Vogt A. Follicular transport route–research progress and future perspectives. Eur J Pharm Biopharm. 2009;71:173–80.
33. Jung S, Patzelt A, Otberg N, Thiede G, Sterry W, Lademann J. Strategy of topical vaccination with nanoparticles. J Biomed Opt. 2009;14:021001.
34. Messenger AG. Alopecia areata. Eur J Dermatol. 2006;16:537–42.
35. Küchler S, Radowski MR, Blaschke T, Dathe M, Plendl J, Haag R, *et al.* Nanoparticles for skin penetration enhancement–a comparison of a dendritic core-multishell-nanotransporter and solid lipid nanoparticles. Eur J Pharm Biopharm. 2009;71:243–50.
36. Hillaireau H, Couvreur P. Nanocarriers' entry into the cell: relevance to drug delivery. Cell Mol Life Sci. 2009;66:2873–96.
37. Lu W, Sun Q, Wan J, She Z, Jiang XG. Cationic albumin-conjugated pegylated nanoparticles allow gene delivery into brain tumors *via* intravenous administration. Cancer Res. 2006;66:11878–87.
38. Lv Q, Yu A, Xi Y, Li H, Song Z, Cui J, *et al.* Development and evaluation of penciclovir-loaded solid lipid nanoparticles for topical delivery. Int J Pharm. 2009;372:191–8.
39. Alvarez-Román R, Naik YN, Fessi H, Guy RH. Visualization of skin penetration using confocal laser scanning microscopy. Eur J Pharm Biopharm. 2004;58:301–16.
40. Otberg N, Richter H, Schaefer H, Blume-Peytavi U, Sterry W, Lademann J. Variations of hair follicle size and distribution in different body sites. J Invest Dermatol. 2004;122:14–9.
41. Frum Y, Bonner MC, Eccleston GM, Meidan VM. The influence of drug partition coefficient on follicular penetration: *in vitro* human skin studies. Eur J Pharm Sci. 2007;30:280–7.
42. Trauer S, Patzelt A, Otberg N, Knorr F, Rozycki C, Balizs G, *et al.* Permeation of topically applied caffeine through human skin–a comparison of *in vivo* and *in vitro* data. Br J Clin Pharmacol. 2009;68:181–6.